Geochemical Perspectives Letters

^{182}W evidence for core-mantle interaction in the source of mantle plumes

H. Rizo[1*], D. Andrault[2], N.R. Bennett[3], M. Humayun[4], A. Brandon[5], I. Vlastelic[2], B. Moine[6], A. Poirier[7], M.A. Bouhifd[2], D.T. Murphy[8]

OPEN ACCESS

doi: 10.7185/geochemlet.1917

Abstract

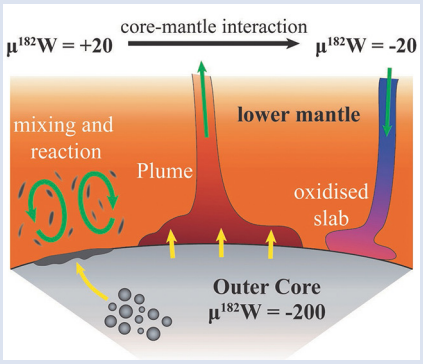

Tungsten isotopes are the ideal tracers of core-mantle chemical interaction. Given that W is moderately siderophile, it preferentially partitioned into the Earth's core during its segregation, leaving the mantle depleted in this element. In contrast, Hf is lithophile, and its short-lived radioactive isotope ^{182}Hf decayed entirely to ^{182}W in the mantle after metal-silicate segregation. Therefore, the ^{182}W isotopic composition of the Earth's mantle and its core are expected to differ by about 200 ppm. Here, we report new high precision W isotope data for mantle-derived rock samples from the Paleoarchean Pilbara Craton, and the Réunion Island and the Kerguelen Archipelago hotspots. Together with other available data, they reveal a temporal shift in the ^{182}W isotopic composition of the mantle that is best explained by core-mantle chemical interaction. Core-mantle exchange might be facilitated by diffusive isotope exchange at the core-mantle boundary, or the exsolution of W-rich, Si-Mg-Fe oxides from the core into the mantle. Tungsten-182 isotope compositions of mantle-derived magmas are similar from 4.3 to 2.7 Ga and decrease afterwards. This change could be related to the onset of the crystallisation of the inner core or to the initiation of post-Archean deep slab subduction that more efficiently mixed the mantle.

Received 1 April 2019 | Accepted 17 May 2019 | Published 20 June 2019

Letter

Deep-rooted upwelling mantle plumes are potential candidates for carrying geochemical evidence of chemical interaction between the liquid outer core and the base of the mantle. Ocean island basalts (OIB), erupted at hotspots, are the surface expression of these mantle plumes. While the He and Os isotope compositions and Fe/Mn ratios of these magmas have been interpreted as possible evidence for core-mantle exchange (*e.g.*, Walker *et al.*, 1995; Brandon *et al.*, 1998; Porcelli and Halliday, 2001; Humayun *et al.*, 2004; Bouhifd *et al.*, 2013), other interpretations have also been invoked (*e.g.*, Sobolev *et al.*, 2007; Lassiter, 2006; Luguet *et al.*, 2008).

Strong evidence for core-mantle interaction may come from the short-lived ^{182}Hf-^{182}W system. With a half-life of 8.9 Ma (Vockenhuber *et al.*, 2004), ^{182}Hf decayed into ^{182}W during the first ~50 Myr of the solar system's history. Since Hf is a lithophile element, it is concentrated in the silicate portion of the Earth. In contrast, W partitions preferentially into metal, and mass balance calculations suggest that ~90 % of the Earth's W resides in the core (McDonough, 2003). The difference in the W isotopic composition of the Earth's mantle and chondritic meteorites implies that the W-rich core has a ^{182}W/^{184}W ratio ~200 ppm lower than the mantle (*e.g.*, Kleine *et al.*, 2009). Therefore, chemical exchange between the core and the source of mantle plumes could be detectable in the ^{182}W/^{184}W ratio of OIB.

The samples studied here are plume-related volcanic rocks from the Réunion Island and the Kerguelen Archipelago hotspots, the certified reference material Hawaiian basalt BHVO-2, as well as samples from the ~3.475 Ga Mount Ada Basalts of the Pilbara Craton (samples and analytical methods are described in the Supplementary Information). The ^{182}W isotope compositions of these samples are presented as μ^{182}W values in Table 1 and Figure 1, which are deviations in ppm from the W isotopic composition of the terrestrial standard

1. Department of Earth Sciences, Carleton University, Ottawa-Carleton Geoscience Centre, Ottawa, ON, K1S 5B6, Canada
2. Laboratoire Magmas et Volcans, Université Clermont-Auvergne, CNRS, IRD, OPGC, Clermont-Ferrand, France
3. Department of Earth and Planetary Sciences, University of California, Davis, CA 95616, USA
4. Department of Earth, Ocean and Atmospheric Science, and National High Magnetic Field Laboratory, Florida State University, Tallahassee, FL 32310, USA
5. Department of Earth and Atmospheric Sciences, University of Houston, Houston, TX 77204, USA
6. Université Lyon, UJM Saint-Etienne, UCA, IRD, CNRS, Laboratoire Magmas et Volcans UMR 6524, Saint Etienne, France
7. Département des Sciences de la Terre et de l'atmosphère, Geotop-Université du Québec à Montréal, Montreal, QC, H2X 3Y7, Canada
8. Queensland University of Technology, Brisbane, Queensland, Australia
* Corresponding author (e-mail: Hanika.Rizo@carleton.ca)

(assumed $\mu^{182}W = 0$). All plume-related samples analysed here yield negative $\mu^{182}W$ values ranging from -5.2 ± 3.7 to -20.2 ± 5.1, including BHVO-2, which yields an average $\mu^{182}W$ of -6.6 ± 1.9, consistent with previous reports (Willbold *et al.*, 2011; Mundl *et al.*, 2017; Kruijer and Kleine, 2018; Mei *et al.*, 2018). In contrast, the ~3.475 Ga Mt. Ada Basalts samples yield positive $\mu^{182}W$ values of +15.3 ± 4.6 and +13.1 ± 4.1, in the same range as most Hadean and Eoarchean mantle-derived rocks. Deviations measured in $\mu^{182}W$ are not associated with deviations in $\mu^{183}W$, confirming that ^{182}W variability is not the result of nuclear field shift effects (Figs. S-1 and S-2).

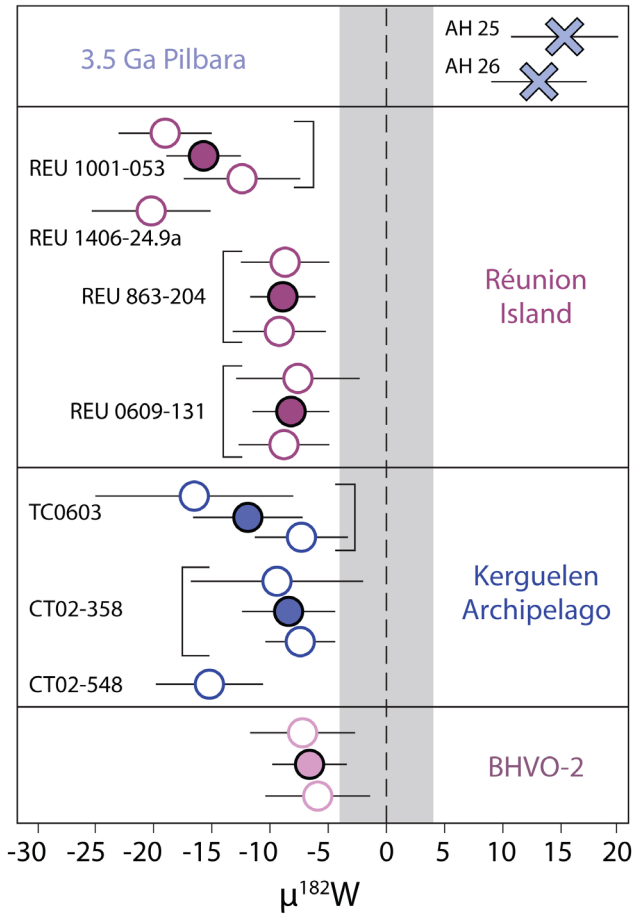

Figure 1 $^{182}W/^{184}W$ data obtained in this study shown as $\mu^{182}W$ values. Open symbols are individual analysis of samples and filled symbols show the average of the different duplicates. Errors on individual measurements shown are 2 standard error (2 s.e.) and propagated uncertainties are shown for averages. The shaded area represents the reproducibility obtained (2 s.d.) on repeated measurements of the Alfa Aesar W standard.

Coupled with other high precision W isotope studies of mantle-derived rocks, the data reveal that the ^{182}W isotopic composition in the Hadean-Archaean mantle was different from the modern mantle (Fig. 2). With the exception of the ~3.55 Ga Schapenburg komatiites, Hadean to Archean volcanism sampled a mantle characterised by ^{182}W excesses of +5 to +20 ppm. In contrast, the mantle accessed by modern mantle-plume magmatism is characterised by ^{182}W anomalies from +5 to -20 ppm. The lavas from the Canary Islands are the only OIB to display resolvable ^{182}W excesses, however, this hotspot seems to originate at shallower depths (King and Ritsema, 2000; Courtillot *et al.*, 2003) and various geochemical tracers suggest these magmas were contaminated by the ancient continental root (*e.g.*, Thirlwall *et al.*, 1997).

Several processes have been proposed to explain the cause of ^{182}W variability. None of these processes, however, seems to explain all geochemical observations satisfactorily. For example, excesses in ^{182}W observed in ancient rock samples could arise if they derived from mantle sources that remained partially isolated from the incorporation, after core formation, of meteoritic material (*e.g.*, Willbold *et al.*, 2011). This late-accreted material is assumed to possess $\mu^{182}W$ ~ -200, and its gradual homogenisation into the mantle would have decreased its $\mu^{182}W$ with time. Late accretion of ~0.5 wt. % of the Earth has also been invoked to explain the higher than expected highly siderophile element (HSE; Re, Os, Ir, Ru, Pt, Pd) abundances in Earth's mantle (*e.g.*, Chou *et al.*, 1978; Walker, 2009). Therefore, variability of ^{182}W is expected to correlate with HSE source abundances. Yet, it rarely does, and the HSE depleted Schapenburg samples even indicate the opposite relationship (Puchtel *et al.*, 2016). Estimating HSE abundances of mantle sources is, however, complicated since these elements are controlled by sulphides, whose partial melting behaviour is very complex.

Another proposed process is that early (<50 Ma) silicate differentiation, following crystallisation of a magma ocean, could have also created ^{182}W variability. Since W is more incompatible than Hf (Shearer and Righter, 2003), early differentiated reservoirs will be characterised by fractionated Hf/W ratios and develop excesses and deficits in ^{182}W. Silicate differentiation in the first 50 Ma of Earth's history should have also affected the short-lived ^{146}Sm-^{142}Nd isotope system ($t_{1/2}$ = 103 Ma; Marks *et al.*, 2014). Coupled ^{142}Nd and ^{182}W anomalies in the ancient rock record, however, are not ubiquitous and most modern mantle rocks measured so far exhibit ^{142}Nd variations that deviate by less than 5 ppm from the terrestrial standard (Fig. S-3).

While the scenarios discussed above might explain some of the ^{182}W anomalies detected in the rock record, the temporal shift observed in the W isotopic composition of the mantle seems to reflect one predominating process. Chemical interaction between the core and the mantle sources of plumes could be such a process. Core-mantle interaction does not affect lithophile elements such as Nd, and is thus compatible with the observed lack of coupling between ^{182}W and ^{142}Nd. Furthermore, the correlations between ^{182}W and $^{3}He/^{4}He$ ratios (Mundl *et al.*, 2017) and Fe/Mn ratios (Fig. S-4) could corroborate this process, since both He and Fe/Mn have also been proposed as tracers of core-mantle interaction (Porcelli and Halliday, 2001; Humayun *et al.*, 2004; Bouhifd *et al.*, 2013). In this scenario, the Earth's mantle, initially characterised by a maximum $\mu^{182}W$ value of +20, was subject to core addition that created domains with $\mu^{182}W$ values as low as -20. The most negative $\mu^{182}W$ values measured in OIB constrain the maximum core contribution to their sources to ~0.8 wt. %, calculated by mass balance assuming a core $\mu^{182}W$ value of -200 (Kleine *et al.*, 2009) and W concentration of ~500 ppb (McDonough, 2003).

Diffusive isotope exchange of W at the core-mantle boundary (CMB) is one of the plausible mechanisms of core-mantle interaction (Fig. 3). At CMB conditions, grain boundary diffusion experiments indicate W can diffuse over distances of 1-10 km in the mantle over 100 Myr (Hayden and Watson, 2007) and even higher diffusion rates may arise from the presence of partially molten silicates at the CMB (*e.g.*, Andrault *et al.*, 2014; Yuan and Romanowicz, 2017). Hayden and Watson (2007) also determined the grain boundary diffusivity of the HSE, and concluded that these elements are also susceptible to 'leaking' from the core over geological timescales. The high concentrations of HSE in the core relative to the mantle mean that even a small flux of HSEs from the core should result in coupling between $\mu^{182}W$ and HSE abundances in mantle-derived rocks. As discussed above, mantle-derived rocks with negative $\mu^{182}W$ values do not possess HSE enrichments,

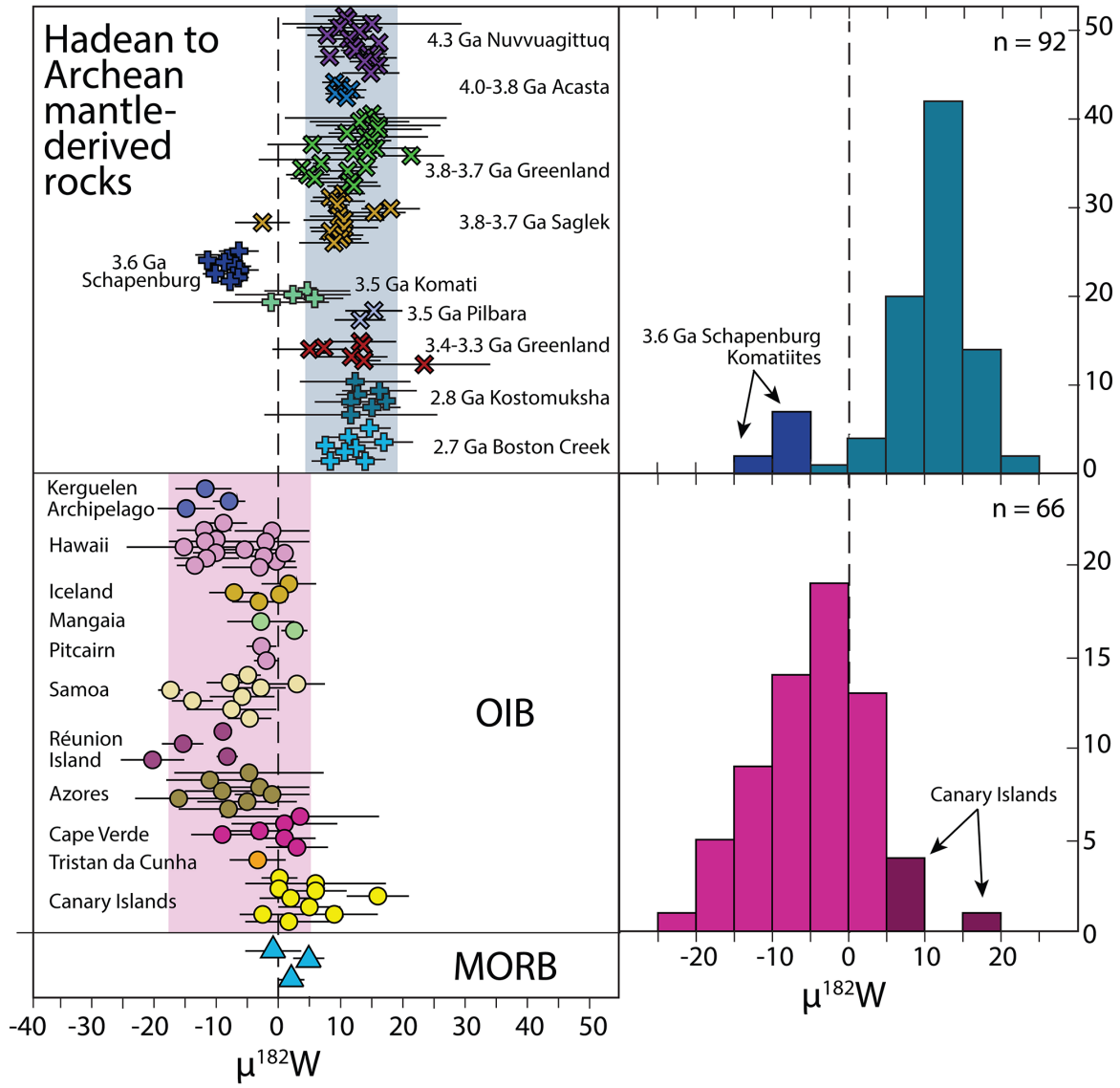

Figure 2 Compilation of all existing $^{182}W/^{184}W$ data shown as $\mu^{182}W$ values. Hadean and Archean mantle-derived rocks are organised in order of their age, with the oldest at the top and the youngest at the bottom. Shaded areas show the average $\mu^{182}W$ values ± 2 s.d. for Hadean-Archean and OIB samples. OIB: Ocean Island Basalts. MORB: Mid-Ocean Ridge Basalts. Data sources: Willbold *et al.*, 2011, 2015; Touboul *et al.*, 2012, 2014; Liu *et al.*, 2016; Puchtel *et al.*, 2016, 2018; Rizo *et al.*, 2016a,b; Dale *et al.*, 2017; Mundl *et al.*, 2017; Kruijer and Kleine, 2018; Mei *et al.*, 2018; Reimink *et al.*, 2018; and this study.

perhaps suggesting that this is not the primary mechanism of core-mantle interaction. However, relating HSE concentrations in mantle-derived rocks to the composition of their source regions is challenging and means we cannot rule out diffusion as a viable mechanism.

Core-mantle interaction could be also a consequence of Si-Mg-Fe oxide exsolutions from the core (Badro *et al.*, 2016; O'Rourke and Stevenson, 2016; Hirose *et al.*, 2017) (Fig. 3). Our experimental results show that these oxides can efficiently incorporate W in their structure without the accompanying HSE (Supplementary Information; Figs. S-5 and S-6). These exsolutions are expected to form by simple secular core cooling, since the solubility of oxides in liquid iron decreases with decreasing temperature (Badro *et al.*, 2016; O'Rourke and Stevenson, 2016; Hirose *et al.*, 2017). Additional to core cooling, the crystallisation of the inner core likely led to higher oxygen concentrations in the outer liquid core and increased Si-Mg-Fe oxide precipitation, since oxygen is not easily incorporated into solid iron (Alfè *et al.*, 2002). More oxidising conditions in the outer core decreases the affinity of W for the liquid metal (Righter and Ghiorso, 2012; Wade *et al.*, 2012), inducing the extraction of W from the core and its incorporation into the mantle.

Regardless of the exact mechanism of core-mantle interaction, a key observation to consider is that the mantle between 4.3 Ga and 2.7 Ga seems to be characterised by constant $\mu^{182}W$ values, which have decreased in the modern mantle (Fig. 2). This broad distinction in $\mu^{182}W$ *vs.* age could imply a change in mantle dynamics after the Archean. Slab subduction of oxidised material into the deep mantle might have induced W disequilibrium at the CMB by increasing its fO_2 (van der Hilst and Kárason, 1999). Since W adopts a high valence (4+ to 6+) in silicates, increasing the fO_2 at the CMB decreases its siderophile behaviour (*e.g.*, Righter and Ghiorso, 2012; Wade *et al.*, 2012), favouring its extraction from the core and incorporation in the lower mantle. Deep slab subduction might have also played a role in scavenging material from the CMB. Alternatively, the change of $\mu^{182}W$ values in the post-Archaean mantle could be related to the crystallisation of the inner core. Large experimental uncertainties on thermal conductivity values of liquid iron in the outer core limit our understanding of inner core crystallisation. If changes in the $\mu^{182}W$ signature of deep mantle plumes are related to the onset of inner core segregation, $\mu^{182}W$ could be used as an alternative tool to study this process.

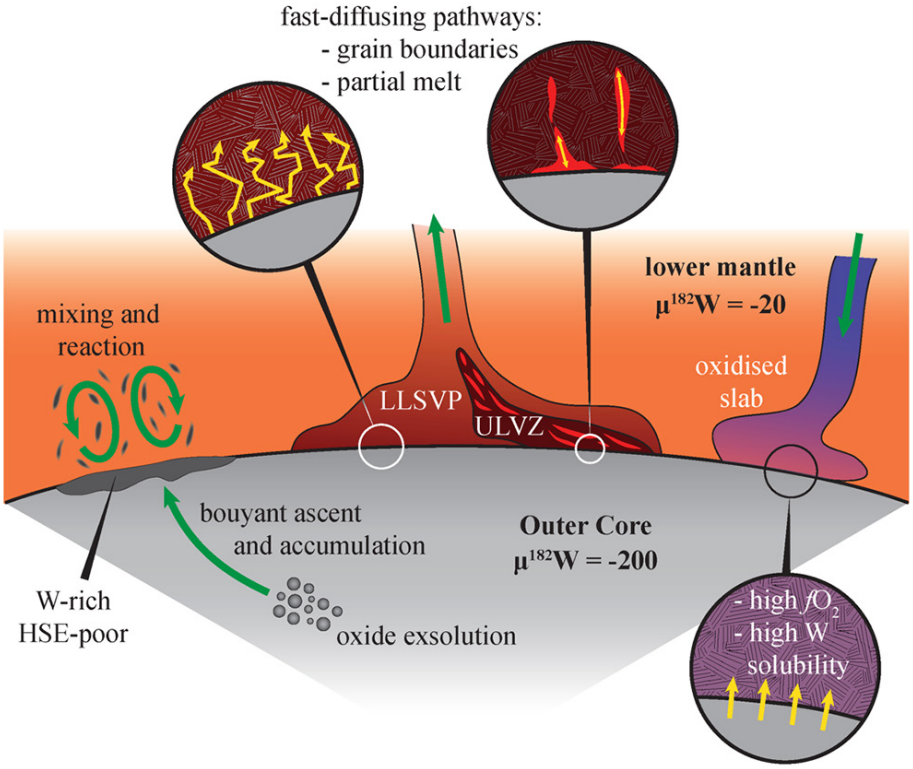

Figure 3 Schematic cartoon showing possible processes for core-mantle chemical interaction.

Table 1 Tungsten isotope results for rock samples from the Pilbara Craton, the Kerguelen Archipelago, Réunion Island and the Hawaiian basalt BHVO-2.

Location	Sample	$\mu^{182}W$	$\mu^{183}W$
Réunion Island	REU 1001-053	-19.0 ± 4.0	-3.3 ± 3.5
	REU 1001-053 duplicate	-12.4 ± 5.0	-1.6 ± 4.0
	REU 1001-053 average	-15.7 ± 3.2	-2.4 ± 2.7
	REU 1406-24.9a	-20.2 ± 5.1	-5.8 ± 4.7
	REU 863-204	-8.7 ± 3.8	0.7 ± 3.3
	REU 863-204 duplicate	-9.2 ± 4.0	-0.8 ± 3.4
	REU 863-204 average	-8.9 ± 2.8	-0.1 ± 2.4
	REU 0609-131	-7.6 ± 5.3	0.4 ± 4.7
	REU 0609-131 duplicate	-8.8 ± 3.9	4.0 ± 3.2
	REU 0609-131 average	-8.2 ± 3.3	2.2 ± 2.9
Kerguelen Plateau	TC0603	-16.5 ± 8.5	-3.1 ± 5.8
	TC0603 duplicate	-7.3 ± 4.0	2.1 ± 3.4
	TC0603 average	-11.9 ± 4.7	-0.5 ± 3.3
	CT02-358	-9.4 ± 7.4	-2.8 ± 7.2
	CT02-358 duplicate	-7.4 ± 3.0	1.9 ± 2.6
	CT02-358 average	-8.4 ± 4.0	-0.4 ± 3.8
	CT02-548	-15.2 ± 4.6	1.1 ± 3.7
Hawaii	BHVO-2	-7.2 ± 4.5	-0.9 ± 3.9
	BHVO-2 duplicate	-5.9 ± 4.5	4.3 ± 3.9
	BHVO-2 average	-6.6 ± 3.2	1.7 ± 2.8
Pilbara Craton	AH-25	15.3 ± 4.6	2.4 ± 3.7
	AH-26	13.1 ± 4.1	5.2 ± 3.5

$\mu^{X}W$ values ($\mu^{X}W = ([(^{X}W/^{184}W)_{sample}/(^{X}W/^{184}W)_{standard}]-1) \times 10^{6}$) are relative deviations of the W isotope composition of the samples from the Alfa Aesar W terrestrial standard in ppm. The standard was measured repeatedly between samples and yields a reproducibility on the $^{182}W/^{184}W$ ratio of 4.7 ppm (2 s.d., n = 11). Duplicates are measurements from different rock digestions. Errors on individual measurements are 2 standard error (2 s.e.) and averages show the propagated uncertainties on the average of multiple duplicates.

Acknowledgements

This manuscript was improved after insightful comments from G. Pearson and four anonymous reviewers and the editor, A. Luguet. We appreciate helpful discussions with R.W. Carlson, R. Walker and J. O'Neil, and discussions related to analytical protocols with G. Quitté, G. Archer and J. Blenkinsop. We thank L. Bouvier for her participation in the beginning of this project, and S. Zhang for assistance with TIMS, and N. DeSilva and S. Mohanty for assistance with ICP-MS facilities. We also thank the Geological Survey of Western Australia and R. Hepple for assistance with collection of the Pilbara Craton samples. This research was supported by a Natural Sciences and Engineering Research Council of Canada (NSERC) Discovery grant to H. Rizo (RGPIN-2015-03982), and by the Fonds de Recherche Nature et Technologies (FRQNT) start up programme for new university researchers.

Editor: Ambre Luguet

Additional Information

Supplementary Information accompanies this letter at http://www.geochemicalperspectivesletters.org/article1917.

Cite this letter as: Rizo, H., Andrault, D., Bennett, N.R., Humayun, M., Brandon, A., Vlastelic, I., Moine, B., Poirier, A., Bouhifd, M.A., Murphy, D.T. (2019) ^{182}W evidence for core-mantle interaction in the source of mantle plumes. *Geochem. Persp. Let.* 11, 6–11.

References

Alfè, D., Price, G.D., Gillan, M.J. (2002) Iron under Earth's core conditions: Liquid-state thermodynamics and high-pressure melting curve from ab initio calculations. *Physical Review B* 65, 16511.

Andrault, D., Pesce, G., Bouhifd, M.A., Bolfan-Casanova, N., Hénot, J.M., Mezouar, M. (2014) Melting of subducted basalt at the core-mantle boundary. *Science* 344, 892-895.

Badro, J., Siebert, J., Nimmo, F. (2016) An early geodynamo driven by exsolution of mantle components from Earth's core. *Nature* 536, 326.

Brandon, A.D., Walker, R.J., Morgan, J.W., Norman, M.D., Prichard, H.M. (1998) Coupled ^{186}Os and ^{187}Os evidence for core-mantle interaction. *Science* 280, 1570-1573.

Bouhifd, M.A., Jephcoat, A.P., Heber, V.S., Kelley, S.P. (2013) Helium in an early Earth's core. *Nature Geoscience* 6, 982-986.

Chou, C.L. (1978) Fractionation of siderophile elements in the Earth's upper mantle. *Proceedings of the 9th Lunar and Planetary Science Conference* 1, 219-230.

Courtillot, V., Davaille, A., Besse, J., Stock, J. (2003) Three distinct types of hotspots in the Earth's mantle. *Earth and Planetary Science Letters* 205, 295-308.

Dale, C.W., Kruijer, T.S., Burton, K.W. (2017) Highly siderophile element and ^{182}W evidence for a partial late veneer in the source of 3.8 Ga rocks from Isua, Greenland. *Earth and Planetary Science Letters* 458, 394-404.

Hayden, L.A., Watson, E.B. (2007) A diffusion mechanism for core–mantle interaction. *Nature* 450, 709.

Hirose, K., Morard, G., Sinmyo, R., Umemoto, K., Hernlund, J., Helffrich, G., Labrosse, S. (2017) Crystallization of silicon dioxide and compositional evolution of the Earth's core. *Nature* 543, 99.

Humayun, M., Qin, L., Norman, M.D. (2004) Geochemical evidence for excess iron in the mantle beneath Hawaii. *Science* 306, 91-94.

Kleine, T., Touboul, M., Bourdon, B., Nimmo, F., Mezger, K., Palme, H., Jacobsen, S.B., Yin, Q.-Z., Halliday, A.N. (2009) Hf–W chronology of the accretion and early evolution of asteroids and terrestrial planets. *Geochimica et Cosmochimica Acta* 73, 5150-5188.

King, S.D., Ritsema, J. (2000) African hot spot volcanism: small-scale convection in the upper mantle beneath cratons. *Science* 290, 1137-1140.

Kruijer, T.S., Kleine, T. (2018) No ^{182}W excess in the Ontong Java Plateau source. *Chemical Geology* 485, 24-31.

Lassiter, J.C. (2006) Constraints on the coupled thermal evolution of the Earth's core and mantle, the age of the inner core, and the origin of the ^{186}Os/^{188}Os "core signal" in plume-derived lavas. *Earth and Planetary Science Letters* 250, 306-317.

Liu, J., Touboul, M., Ishikawa, A., Walker, R.J., Pearson, D.G. (2016) Widespread tungsten isotope anomalies and W mobility in crustal and mantle rocks of the Eoarchean Saglek Block, northern Labrador, Canada: Implications for early Earth processes and W recycling. *Earth and Planetary Science Letters* 448, 13-23.

Luguet, A., Pearson, D.G., Nowell, G.M., Dreher, S.T., Coggon, J.A., Spetsius, Z.V., Parman, S. W. (2008) Enriched Pt-Re-Os isotope systematics in plume lavas explained by metasomatic sulfides. *Science* 319, 453-456.

Marks, N.E., Borg, L.E., Hutcheon, I.D., Jacobsen, B., Clayton, R.N. (2014) Samarium–neodymium chronology and rubidium–strontium systematics of an Allende calcium–aluminum-rich inclusion with implications for ^{146}Sm half-life. *Earth and Planetary Science Letters* 405, 15-24.

McDonough, W.F. (2003) Compositional model for the Earth's core. *Treatise on geochemistry* 2, 568.

Mei, Q.F., Yang, J.H., Yang, Y.H. (2018) An improved extraction chromatographic purification of tungsten from a silicate matrix for high precision isotopic measurements using MC-ICPMS. *Journal of Analytical Atomic Spectrometry* 33, 569-577.

Mundl, A., Touboul, M., Jackson, M.G., Day, J.M., Kurz, M.D., Lekic, V., Helz, R.T., Walker, R.J. (2017) Tungsten-182 heterogeneity in modern ocean island basalts. *Science* 356, 66-69.

O'Rourke, J.G., Stevenson, D.J. (2016) Powering Earth's dynamo with magnesium precipitation from the core. *Nature* 529, 387.

Porcelli, D., Halliday, A.N. (2001) The core as a possible source of mantle helium. *Earth and Planetary Science Letters* 192, 45-56.

Puchtel, I.S., Blichert-Toft, J., Touboul, M., Horan, M.F., Walker, R.J. (2016) The coupled ^{182}W-^{142}Nd record of early terrestrial mantle differentiation. *Geochemistry, Geophysics, Geosystems* 17, 2168-2193.

Puchtel, I.S., Blichert-Toft, J., Touboul, M., Walker, R.J. (2018) ^{182}W and HSE constraints from 2.7 Ga komatiites on the heterogeneous nature of the Archean mantle. *Geochimica et Cosmochimica Acta* 228, 1-26.

Reimink, J.R., Chacko, T., Carlson, R.W., Shirey, S.B., Liu, J., Stern, R.A., Bauer, A.M., Pearson, D.G., Heaman, L.M. (2018) Petrogenesis and tectonics of the Acasta Gneiss Complex derived from integrated petrology and ^{142}Nd and ^{182}W extinct nuclide-geochemistry. *Earth and Planetary Science Letters* 494, 12-22.

Righter, K., Ghiorso, M.S. (2012) Redox systematics of a magma ocean with variable pressure-temperature gradients and composition. *Proceedings of the National Academy of Sciences* 109, 11955-11960.

Rizo, H., Walker, R.J., Carlson, R.W., Horan, M.F., Mukhopadhyay, S., Manthos, V., Francis, D., Jackson, M.G. (2016a) Preservation of Earth-forming events in the tungsten isotopic composition of modern flood basalts. *Science* 352, 809-812.

Rizo, H., Walker, R.J., Carlson, R.W., Touboul, M., Horan, M.F., Puchtel, I.S., Boyet, M., Rosing, M.T. (2016b) Early Earth differentiation investigated through ^{142}Nd, ^{182}W, and highly siderophile element abundances in samples from Isua, Greenland. *Geochimica et Cosmochimica Acta* 175, 319-336.

Shearer, C.K., Righter, K. (2003) Behavior of tungsten and hafnium in silicates: a crystal chemical basis for understanding the early evolution of the terrestrial planets. *Geophysical Research Letters* 30, 7-1.

Sobolev, A.V., Hofmann, A.W., Kuzmin, D.V., Yaxley, G.M., Arndt, N.T., Chung, S.L., Danyushevsky, L.V., Elliott, T., Frey, F.A., Garcia, M.O., Gurenko, A.A., Kamenetsky, V.S., Kerr, A.C., Krivolutskaya, N.A., Matvienkov, V.V., Nikogosian, I.K.,

Rocholl, A., Sigurdsson, I.A., Sushchevskaya, N.M., Teklay, M. (2007) The amount of recycled crust in sources of mantle-derived melts. *Science* 316, 412-417.

Thirlwall, M.F., Jenkins, C., Vroon, P.Z., Mattey, D.P. (1997) Crustal interaction during construction of ocean islands: Pb-Sr-Nd-O isotope geochemistry of the shield basalts of Gran Canaria, Canary Islands. *Chemical Geology* 135, 233-262.

Touboul, M., Puchtel, I.S., Walker, R.J. (2012) ^{182}W evidence for long-term preservation of early mantle differentiation products. *Science* 335, 1065-1069.

Touboul, M., Liu, J., O'Neil, J., Puchtel, I.S., Walker, R.J. (2014) New insights into the Hadean mantle revealed by ^{182}W and highly siderophile element abundances of supracrustal rocks from the Nuvvuagittuq Greenstone Belt, Quebec, Canada. *Chemical Geology* 383, 63-75.

van der Hilst, R.D., Kárason, H. (1999) Compositional heterogeneity in the bottom 1000 kilometers of Earth's mantle: toward a hybrid convection model. *Science* 283, 1885-1888.

Vockenhuber, C., Oberli, F., Bichler, M., Ahmad, I., Quitté, G., Meier, M., Halliday, A.N., Lee, D.-C., Kutschera, W., Steier, P., Gehrke, R.J., Helmer, R.G. (2004) New Half-Life Measurement of Hf-182: Improved Chronometer for the Early Solar System. *Physical Review Letters* 93, 172501.

Walker, R.J. (2009) Highly siderophile elements in the Earth, Moon and Mars: update and implications for planetary accretion and differentiation. *Chemie der Erde-Geochemistry* 69, 101-125.

Walker, R.J., Morgan, J.W., Horan, M.F. (1995) Osmium-187 enrichment in some plumes: evidence for core-mantle interaction?. *Science* 269, 819-822.

Wade, J., Wood, B.J., Tuff, J. (2012) Metal–silicate partitioning of Mo and W at high pressures and temperatures: evidence for late accretion of sulphur to the Earth. *Geochimica et Cosmochimica Acta* 85, 58-74.

Willbold, M., Elliott, T., Moorbath, S. (2011) The tungsten isotopic composition of the Earth's mantle before the terminal bombardment. *Nature* 477, 195.

Willbold, M., Mojzsis, S.J., Chen, H.W., Elliott, T. (2015) Tungsten isotope composition of the Acasta Gneiss Complex. *Earth and Planetary Science Letters* 419, 168-177.

Yuan, K., Romanowicz, B. (2017) Seismic evidence for partial melting at the root of major hot spot plumes. *Science* 357, 393-397.

Geochemical Perspectives Letters

^{182}W evidence for core-mantle interaction in the source of mantle plumes

H. Rizo, D. Andrault, N.R. Bennett, M. Humayun, A. Brandon, I. Vlastelic, B. Moine, A. Poirier, M.A. Bouhifd, D.T. Murphy

Supplementary Information

The Supplementary Information includes:

- 1. Sample Description
- 2. Analytical Methods for W Concentrations and Isotope Measurements
- 3. Correlations Between ^{182}W and ^{3}He/^{4}He and Fe/Mn Ratios
- 4. Evidence for W Solubility in Exsolved Oxides and Decoupling of W and HSE Abundances
- Tables S-1 to S-4
- Figures S-1 to S-6
- Supplementary Information References

1. Sample Description

1.1. Réunion Island Samples

Réunion Island samples are fresh lavas produced during the recent (1986-2010) activity of the Piton de la Fournaise volcano. Sample REU 863-204 is from the March 1986 eruption, which propagated along the South-East rift zone. This rock sample was collected at Ravine Takamaka (880 m elevation). Sample REU 0609-131 was collected during the August 2006 summit eruption, which occurred entirely within the Dolomieu crater at 2500 m. The molten lava was quenched in water immediately after sampling. Samples REU 1001-053 and REU 1406-24.9a are lapilli emitted on the upper flanks of the Dolomieu Crater during the January 2010 and June 2014 eruptions, respectively. Sample REU 863-204 is poorly phyric, whereas the other three samples are mostly glassy. A detailed description of the composition of the samples is provided in Vlastélic *et al.* (2009; 2013; 2018) and Gurioli *et al.* (2017) and only the main characteristics are given here. Major element compositions are transitional between alkali basalts and tholeiites, as are most Réunion Island shield lavas. The samples have 6.5-8.0 wt. % MgO, 67-134 ppm Ni, and 54-270 ppm Cr, and belong to a dominant, homogeneous lava group often named "Steady State Basalts". The ^{87}Sr/^{86}Sr (0.704136-0.704200) and ^{206}Pb/^{204}Pb (18.901-18.930) ratios of the samples plot in the middle of the narrow isotope field of Réunion Island samples.

1.2. Kerguelen Archipelago Samples

Since the Cretaceous Kerguelen Plateau basalts are known to have assimilated shallow-level continental crust materials (*e.g.*, Ingle *et al.*, 2003), all the samples studied here were collected from the Kerguelen Archipelago, which is the Cenozoic part of the Plateau. Some of these more recent lavas might reflect some degree of mixing with depleted upper mantle or assimilated overlying

Cretaceous lithosphere, but given the low expected W concentration of these contaminants, the Kerguelen Archipelago samples remain the best candidates for this study. Samples were collected during field seasons of summer 2002 (CarbonatoKer program) and 2006 (DyLIOKer program of the Institut Polaire Français). All of the samples studied here are high-MgO basalts containing olivine and clinopyroxene phenocrysts. These rock types represent the less differentiated liquids, with little to no crustal contamination, and are the most representative of the mantle plume signature (minimum mixing with Indian mid ocean ridge basalts and/or lithospheric components).

Kerguelen sample CT02-358 comes from Monts Aubert de la Rue (S49°36′42″ E69°40′50″), with estimated emplacement age between 18-20 Ma. Sample CT02-548 is a phonolite collected in Val Phonolite (south west of Presqu'ile Ronarc'h, S49°35′52″ E70°05′25″) with eruption dates between 6-12 Ma. Sample TC06-03 is from the Peninsula of Loranchet (Port Léontine S48°58′54″ E69°59′21″), with an estimated emplacement age between 19-24 Ma. Similar samples (CT02-373, CT02-376 and RR08-123) from the same locations were analysed for He isotope compositions and yielded R/Ra ratios between 10.6 and 12.46 (Doucet *et al.*, 2005; 2006).

The three Kerguelen samples were measured here for Pb isotopes at the Geotop laboratoires (Université du Québec à Montréal) and results are given in Table S-1. Measurements were performed on a Nu Plasma II using the Aridus II desolvating membrane as the introduction device. Lead isotope compositions were corrected for mass bias using Tl addition and measuring Pb standard NBS981 as in Woodhead (2002). Reproducibility over 6 years of measurement of our in-house secondary standard solution CGPB-1 shows 2-sigma uncertainties of 204-normalised ratios in the 3rd decimal place, and 4th decimal place for the 206-normalised ones. Full procedural blank yielded 16 pg of common Pb. In Pb-Pb isotopic space, the values obtained here fall onto the array defined by Doucet *et al*. (2005), between NMORB and the Kerguelen plume components.

1.3. Pilbara Craton Samples

Pilbara Craton samples are lower greenschist facies meta-basalts retrieved from coherent outcrops of pillow lavas in the Doolena Gap greenstone belt of the East Pilbara Terrane. The samples are from the 3.475 Ga Mt Ada Basalts of the Warrawoona Group (Kranendonk *et al.*, 2002). Both samples were retrieved from the low strain belt of the western Doolena Gap greenstone belt as defined by Wiemer *et al.* (2016) (AH25; S20°54′20″ E119°43′1″, AH26; S20°54′15″ E119°43′7″). The two outcrops represent lozenges of well-preserved overturned pillow lavas that are surrounded by altered and deformed mafic schists. A detailed description of the stratigraphy and structure of the western Doolena Gap greenstone belt is provided in Wiemer *et al.* (2016).

The samples have a preserved microcrystalline texture defined by altered plagioclase laths. Rare microphenocrysts of plagioclase are present with poorly preserved polysynthetic twinning. Clinopyroxene is rarely present as microcrysts. Equant carbonate features with spinel inclusions are interpreted as pseudomorphs after olivine. Fine-grained epidote, chlorite and carbonate are pervasive throughout the samples.

The two Pilbara Craton samples were measured for major element and trace element chemistry at the Central Analytical Research Facility (CARF), Queensland University of Technology. The results are reported in Table S-2. Major elements were analysed using a WDS XRF Pananalytical Axois 1 kW system. Powdered samples were ignited for *ca*. 3 hours in ceramic crucibles at 950 °C to measure loss on ignition. Trace element analyses were performed with an Agilent 8800 triple quadrupole ICP-MS. 50 mg of sample were dissolved in a mixture of 1.5 mL double distilled HCl, 0.5 mL double distilled HNO_3 and 0.5 mL double distilled HF in PTFE vials using a Milestone bench-top Ultra-wave microwave digestion system. The samples were then transferred to a hotplate at 80-100 °C to evaporate HF in repeated steps of adding HNO_3 and MilliQ, and then washed and centrifuged. Internal standards 9Be, 103Rh, 115In and 209Bi were added to aliquots of the solution for internal standard correction. The geological reference materials W-2 and AGV-2 were analysed as standards.

2. Analytical Methods for W Concentrations and Isotope Measurements

Samples were crushed with metal-free tools to avoid any metal contamination (plastic hammers, ceramic or agate jaw crushers and mortars). All W concentrations (Table S-3) were determined by isotope dilution using a ^{186}W tracer and ~200 mg of rock powder material. Samples were spiked and digested using concentrated HF-HNO_3, followed by repeated dry downs and re-dissolutions in 6N HCl. Once samples were dissolved, W was separated from bulk samples using an anion exchange column with 1ml of AG1-X8 (100-200 mesh) resin. Tungsten concentrations were acquired either using the MC-ICP-MS Nu Plasma II at Geotop laboratories in Montréal or the ICP-MS Triple Quad at the Department of Earth and Environmental Sciences of the University of Ottawa. Total chemistry blanks were typically < 0.2 ng W, representing ~0.3 % of the W measured.

For high-precision W isotope analyses, sample powders were dissolved in order to extract 500-1000 ng of W. Samples were dissolved in concentrated HF-HNO_3 in closed beakers for 4-5 days. Then the samples were dried down and re-dissolved several times in concentrated HNO_3 and then in 6N HCl. Tungsten was then separated from the bulk rock using a similar protocol to the one detailed in Breton and Quitté (2014) and only brief details are given here. Before column chemistry, dissolving the sample in

HF 1N and extracting the supernatant after centrifuging it removes Ca-Mg fluorides, which can incorporate some W. Tungsten was then separated using an anion column filled with 10 mL AG1-X8 (200-400 mesh) resin, and further purified using a column filled with ~ 300 µL of the same AG1-X8 resin. Tungsten recovery using this method was between 80 % and 95 %.

Tungsten isotope compositions were measured on Re filaments as trioxide species (WO_3^-) in the Thermo-Fisher Triton thermal ionisation mass spectrometer (TIMS) at the Department of Earth Sciences of Carleton University in Ottawa. Tungsten oxides were ionised using a mixed solution of La and Gd that acted as an electron emitter and bleeding O_2 into the source, with a source pressure fixed at $1.15e^{-7}$ mbar that facilitates W oxide production. Tungsten isotopes were measured using a similar analytical protocol to the one described in Archer *et al.* (2017), where major oxide species (*e.g.*, $W^{16}O_3$) are measured in Faraday cups electronically connected to 10^{11} ohm resistors, and the low signals $^{186}W^{16}O_2{}^{18}O^-$ and $^{187}Re^{16}O_2{}^{18}O^-$ are measured in Faraday cups connected to 10^{12} ohm resistors. These low signals were used to calculate per-integration oxide corrections to derive the different W isotope ratios. The analyses performed here use a multistatic method consisting of three steps of acquisition with $^{184}W.O_3$, $^{185}Re.O_3$ and $^{187}Re.O_3$ masses placed in the central cup, respectively. Step 1 measures the low signals $^{186}W^{16}O_2{}^{18}O^-$ and $^{187}Re^{16}O_2{}^{18}O^-$ and thus the integration time for this step is 33 s and 12 s for the idle time. Step 2 and step 3 use an 8s integration time and 4 s idle time. Baselines were measured for 1200 s every 7 blocks, and peak centre and lens focus were performed every 3 blocks. Step 1 and 2 are averaged to obtain mean $^{182}W/^{184}W$ and $^{183}W/^{184}W$ ratios. One tungsten isotope measurement represents the average of 560 cycles, measured in 28 blocks of 20 cycles. All tungsten isotope ratios shown in Table S-4 have been corrected for instrumental fractionation using the $^{186}W/^{184}W$ ratio of 0.927670 (Völkening *et al.*, 1991).

Potential analytical problems with the measurement of ^{183}W have been recently reported (Cook and Schönbachler, 2016; Kruijer and Kleine, 2018), where deviations in the stable ^{183}W were measured. These deviations have been attributed to preferential loss of W of the odd mass isotope ^{183}W during the chemical extraction of W from a rock matrix. They suggested that this ^{183}W loss was possibly a result of a nuclear field shift effect that could also affect ^{182}W. None of the samples or standards measured here show resolvable ^{183}W deviations from the isotopic composition of the W terrestrial standard (Figs. S-1 and S-2).

3. Correlations between ^{182}W and $^{3}He/^{4}He$ and Fe/Mn Ratios

Recent high-precision W isotope measurements of rock samples from Hawaii, Samoa and Iceland reported resolvable deficits in ^{182}W compared to terrestrial standard that correlate with $^{3}He/^{4}He$ ratios (Mundl *et al.*, 2017). Furthermore, the Earth's core has been proposed as an important reservoir of He (*e.g.*, Bouhifd *et al.*, 2013; Trieloff and Kunz, 2005), making core-mantle interaction a possible explanation for the ^{182}W *vs.* $^{3}He/^{4}He$ correlation. These ^{182}W observations, however, were difficult to explain by this process since W and Os isotopic compositions were not correlated and the source of these rocks lacked any apparent increase in the abundances of HSE. Estimating HSE source abundances of partial melts is, however, challenging since these elements are affected by several processes including partial melt and fractional crystallisation, as well as sulphide precipitation and mantle oxygen fugacity. Therefore, despite the lack of ^{182}W *vs.* HSE correlation, ^{182}W *vs.* $^{3}He/^{4}He$ characteristics could still translate core-mantle interaction processes.

Core-mantle chemical interaction may also affect Fe abundances in the sources of plumes. This could be detected by precisely measuring the Fe/Mn ratio of plume-related magmas, since Mn is more lithophile than Fe. During partial melting and fractional crystallisation of mantle melts, the Fe/Mn ratio is perturbed less than the FeO abundance. Higher Fe/Mn (10-20 %) in the sources of mantle plumes, particularly Hawaiian lavas, relative to MORB has been documented for several plumes (Humayun *et al.*, 2004; Qin and Humayun, 2008; Vlastélic *et al.*, 2006). During deep (>100 km) partial melting of mantle plumes, pyroxenite residues could also increase the silica contents and Fe/Mn ratios, the latter by preferential retention of Mn in garnet-cpx-rich sources (Sobolev *et al.*, 2007). The constant Fe/Mn ratios from Loihi to Koolau Hawaiian lavas, together with variable Si contents, could argue against pyroxenite residues playing an important role in Fe/Mn variations in Hawaii (Huang *et al.*, 2007).

For each of the locations for which $\mu^{182}W$ data were available, and for the locations for which new $\mu^{182}W$ results are reported here, the available values of Fe/Mn were compiled (Fig. S-4). While FeO and MnO are reported in every major element analysis, two considerations greatly limit the availability of precise Fe/Mn data: (i) rounding error is significant when MnO is reported to only two decimal places, and (ii) alteration affects the Fe/Mn ratio for all but fresh lavas or mineral compositions. Fresh lavas are routinely collected from historic eruptions at Piton de la Fournaise, Reunion, and precise MnO values are available for these lavas (Vlastélic *et al.*, 2006). The mean Fe/Mn value obtained from glasses studied by Vlastélic *et al.* (2006) are identical to the single analysis from Qin and Humayun (2008). Data for Hawaii (Humayun *et al.*, 2004), Iceland and MORB (Qin and Humayun 2008), and the Azores (Humayun, *unpublished*) were based on average values for each of the localities. For the Azores, Fe/Mn data from basalts from Pico Island were taken to match as closely as possible the samples for which $\mu^{182}W$ were available.

4. Evidence for W solubility in Exsolved Oxides and Decoupling of W and HSE Abundances

For Si-Mg-Fe oxides to act as a vehicle for core-mantle exchange of tungsten, they must be able to dissolve this element in appreciable amounts. Furthermore, they must provide a means for fractionating W from the HSEs. There is a paucity of published experiments designed specifically to determine W and HSE partitioning between metallic and oxide melts. However, there is evidence in the literature, and from our own experiments, that FeO-rich oxide melts will both concentrate W and exclude the HSEs relative to Fe-rich metallic melts.

First, we will consider evidence for the solubility of W in exsolved oxides. Figure S-5 displays the run product from a laser-heated diamond anvil cell (LH-DAC) experiment performed at ~24 GPa (cold pressure determined by ruby fluorescence) and 3250 K; conditions where significant amounts of oxygen can dissolve into Fe-rich metallic melt. This experiment was performed with the goal of determining the metal-silicate partitioning of W at high temperature and pressure, but also provides useful information for the present discussion. The starting material was approximately chondritic in composition (C1/C from Thibault and Walter, 1995) that was doped with ~8 wt. % tungsten metal. The sample was heated at beamline 13-ID-D at the Advanced Photon Source using a flat-top fibre laser and quenched by cutting power to the laser. The quenched metallic melt forms a roughly spherical bead at the centre of the heated region, which is mantled by a layer of silicate melt. When the sample is quenched, the decrease in temperature causes saturation of the metallic melt in an FeO-rich oxide phase – now seen as the exsolved darker-grey blebs within the main metal phase. Similar textures were also observed in the W metal-silicate partitioning experiments performed by Shofner *et al.* (2011; 2016). Figure S-5 displays WDS maps for O, Si, Ni, and W for the quenched sample that were acquired with a JEOL 8530F field-emission microprobe located at the Carnegie Institution of Washington, using a 10 kV accelerating voltage and 10 nA beam current. These maps show that W, O, and Si are preferentially concentrated in the exsolved oxide phase relative to the metal, whereas Ni remains concentrated in the metallic melt. These quench textures demonstrate that significant solubility of W in oxide melt is possible, and provide a crude but encouraging hint that W may preferentially partition into this phase over the metallic melt. It is noteworthy that Ni retains its siderophile nature in the presence of an oxide melt, whereas W does not, as some previous partitioning experiments appear to predict these behaviours. Chabot *et al.*, (2015) investigated trace element partitioning between coexisting melts in the Fe-S-O system, in which one melt contains high O concentrations (6–14 wt. %) and the other is essentially O-free. They found that most siderophile elements, including Ni, display O-avoiding behaviour; partitioning more strongly into the O-free melt with increasing O concentrations in the O-rich melt. Tungsten, however, displays the opposite behaviour and partitions more strongly into the O-rich phase as its O content increases. The fact that these trends are reflected in the element distribution of quenched LH-DAC experiments provides encouragement that the qualitative sense of W partitioning between metal and oxide melt is being captured. Furthermore, Shofner *et al.*, (2016) determined the thermal equation of state (EOS) for W and WO_2 and, using the EOS for IW determined by Campbell *et al.*, (2009), demonstrated that for a given T and fO_2, increasing pressure favours the formation of WO_2. At the pressures of the outer core, partitioning of W into exsolved oxide may therefore be enhanced relative to that suggested by our LH-DAC experiment done at only ~24 GPa.

We can also use the results of the Chabot *et al.*, (2015) experiments to assess the likelihood of the HSE being fractionated from W by exsolution of an oxide phase from the core. Unlike W, which displays a preference for oxygen in those experiments, the HSEs universally display O-avoidance behaviour. If, as for Ni and W, the Chabot *et al.*, (2015) experiments provide a pointer to the sense of partitioning between metal and oxide melts, we should expect HSEs to remain concentrated in the metallic melt upon exsolution of an oxide phase. We can again turn to experimental quench textures for support of this prediction.

Fortenfant *et al.* (2003) equilibrated metallic liquids with magnesiowüstite, to investigate the partitioning of Re, Os, and Ni. These experiments were performed at 5 – 10 GPa and 2173 – 2473 K using a multi-anvil apparatus. The authors observed that the quenched metal in these experiments often contained ~2-20 μm blebs of oxygen-bearing liquid iron. The volumetric proportion of these blebs in the metal phase is low, and including them in the analysis of the bulk metal phase had a negligible result on the measured Re and Os concentrations. The authors therefore conclude that the concentrations of Re and Os in the blebs are low (Fortenfant *et al.*, 2003). The metal-magnesiowüstite partition coefficients reported by Fortenfant *et al.*, (2003) may also provide some indication of how HSEs partition between metallic and oxide liquids. The authors find that all three elements they investigated are incompatible in magnesiowustite relative to metal, with incompatibility increasing in the order Ni < Re < Os. This suggests Re and Os will be concentrated in the metal phase during exsolution of an oxide melt. We also note that the incompatibility of Ni in magnesiowustite found by Fortenfant *et al.*, (2003) is in qualitative agreement with our LH-DAC experiment, which shows Ni prefers to remain in the metallic phase.

Bennett *et al.* (2014) presented preliminary results of Soret experiments in the Fe-Ni-O system that were doped with W, Mn, and the HSEs. Samples comprised powdered starting materials encapsulated in alumina and positioned below the hot-spot of a 14/8 multi-anvil assembly, in order to maximise the thermal gradient across the sample. During the experiment, major element gradients develop as a result of heat of transport effects. Trace elements are then redistributed in response to the major element gradient according to their activity-composition relationships. This leads to the alloy at the hot end of the sample being enriched in oxygen. When the sample is quenched, this O-enriched liquid alloy becomes saturated in O and liquid FeO-rich blebs are exsolved. As with the LH-DAC sample in Figure S-5, the composition of these exsolved blebs can provide qualitative clues about the sense of metallic liquid-oxide liquid trace element partitioning. Figure S-6 displays time-resolved LA-ICPMS spectra for one of these

samples, from an experiment performed at 15 GPa and with a temperature at the hot-spot of the assembly of ~2600 K. During analysis, the laser was rastered across the sample surface, to include regions both with and without FeO blebs. Regions of oxide ablation are easily identified in the time-resolved spectra by higher than average counts per second of W and Mn and lower than average counts per second of the HSEs (Figs. S-6a and S-6b respectively). Analyses of the alloy away from the hot end of the sample, where FeO blebs are not observed, show homogeneous time-resolved profiles for all elements. These results qualitatively follow the behaviours observed by Chabot *et al*., (2015) in the Fe-S-O system and support the idea that W is fractionated from the HSEs by metallic liquid-oxide liquid partitioning.

Experiments designed specifically to determine metallic liquid-oxide liquid partitioning for W and the HSEs are clearly needed to rigorously test the suitability of oxide melts for fractionating W from the HSEs. However, we believe that the above observations are a useful starting point for future study and provide evidence that oxides exsolved from the core are a plausible agent for transporting W from the core to the mantle.

Supplementary Tables

Table S-1 Pb isotope compositions for Kerguelen Archipelago samples.

Sample	$^{208}Pb/^{204}Pb$	$^{207}Pb/^{204}Pb$	$^{206}Pb/^{204}Pb$	$^{207}Pb/^{206}Pb$	$^{208}Pb/^{206}Pb$
TC0603	38.805	15.547	18.319	0.8487	2.1184
CT02358	39.175	15.559	18.563	0.8382	2.1105
CT02548	39.021	15.569	18.432	0.8447	2.1171

Table S-2 Major and trace element concentrations for Pilbara samples.

Concentration (wt. %)	AH25	AH26	Concentration (ppm)	AH25	AH26	Concentration (ppm)	AH25	AH26
SiO_2	48.76	47.68	Li	15.24	15.02	U	0.06	0.19
TiO_2	0.91	1.53	Sc	42.54	36.54	Ba	34.59	34.11
Al_2O_3	15.44	13.16	Ti	5575	9981	La	1.97	7.82
Fe_2O_3	10.25	17.12	V	266.7	312.7	Ce	5.89	20.04
MnO	0.17	0.25	Cr	329.2	119.6	Pr	0.97	3.00
MgO	4.24	6.07	Co	52.65	54.07	Nd	5.06	14.42
CaO	6.59	7.89	Ni	153.5	78.46	Sm	1.73	4.08
Na_2O	6.12	1.98	Cu	119.5	119.6	Eu	0.55	1.12
K_2O	0.71	0.41	Zn	90.45	131.3	Gd	2.18	4.54
P_2O_5	0.07	0.13	Rb	9.29	6.17	Tb	0.42	0.81
LOI	7.02	5.70	Sr	56.13	268.3	Dy	2.87	5.24
Total	100.46	102.32	Y	15.18	31.90	Ho	0.62	1.12
			Zr	55.95	111.0	Er	1.80	3.20
			Nb	2.16	6.14	Tm	0.27	0.50
			Mo	0.00	0.14	Yb	1.82	3.17
			Cd	0.00	0.00	Lu	0.27	0.50
			Sb	0.00	0.01	Hf	1.49	2.94
			Cs	0.12	0.11	Ta	0.14	0.35
			Pb	0.64	1.45	Ba	34.59	34.11
			Th	0.22	0.82			

Table S-3 Tungsten concentrations of all samples studied.

Location	Sample	Lithology	W (ppb)
Hawaii	BHVO-2	Basalt	224
Réunion Island	REU 1406-24.9a	Basalt	320
Réunion Island	REU 1001-053	Basalt	317
Réunion Island	REU 863-204	Basalt	364
Réunion Island	REU 0609-131	Basalt	309
Kerguelen Archipelago	TC0603b	Alkaline basalt	589
Kerguelen Archipelago	CT02-358	Alkaline basalt	387
Kerguelen Archipelago	CT02-548	Alkaline basalt	299
Pilbara	AH25	Pillow metabasalt	59
Pilbara	AH26	Pillow metabasalt	96

Table S-4 Detailed W isotope data for the Réunion Island, the Kerguelen Archipelago and the Pilbara Craton samples

Location	Sample	Analytical session	$^{185}Re/^{184}W$	$^{181}Ta/^{184}W$	*Static line 1*		*Static line 2*		*Mean line 1 + line 2*		$\mu^{182}W$	$\mu^{183}W$
					$^{182}W/^{184}W$	$^{183}W/^{184}W$	$^{182}W/^{184}W$	$^{183}W/^{184}W$	$^{182}W/^{184}W$	$^{183}W/^{184}W$		
Réunion Island	REU 1001-053	1	0.28	2.3E-06	0.864870 ± 3	0.467111 ± 1	0.864882 ± 6	0.467116 ± 3	0.864877 ± 3	0.467114 ± 2	-19.0 ± 4.0	-3.3 ± 3.5
	REU 1001-053 duplicate	1	0.26	8.7E-07	0.864870 ± 4	0.467112 ± 2	0.864894 ± 8	0.467119 ± 3	0.864882 ± 4	0.467114 ± 2	-12.4 ± 5.0	-1.6 ± 4.0
	REU 1406-24.9a	1	0.14	8.3E-07	0.864865 ± 5	0.467108 ± 2	0.864887 ± 8	0.467118 ± 4	0.864876 ± 4	0.467113 ± 2	-20.2 ± 5.1	-5.8 ± 4.7
	REU 863-204	2	0.02	-3.7E-06	0.864892 ± 4	0.467119 ± 2	0.864895 ± 5	0.467116 ± 2	0.864893 ± 3	0.467117 ± 2	-8.7 ± 3.8	0.7 ± 3.3
	REU 863-204 duplicate	1	0.14	1.1E-07	0.864881 ± 3	0.467113 ± 1	0.864891 ± 6	0.467118 ± 3	0.864885 ± 3	0.467115 ± 2	-9.2 ± 4.0	-0.8 ± 3.4
	REU 0609-131	2	0.02	-3.7E-06	0.864889 ± 6	0.467118 ± 3	0.864903 ± 6	0.467116 ± 3	0.864894 ± 5	0.467117 ± 2	-7.6 ± 5.3	0.4 ± 4.7
	REU 0609-131 duplicate	1	0.04	3.7E-06	0.864882 ± 3	0.467115 ± 1	0.864891 ± 6	0.467118 ± 3	0.864885 ± 3	0.467117 ± 1	-8.8 ± 3.9	4.0 ± 3.2
Kerguelen Archipelago	TC0603	1	0.07	1.6E-06	0.864875 ± 7	0.467111 ± 3	0.864879 ± 12	0.467116 ± 5	0.864879 ± 7	0.467114 ± 3	-16.5 ± 8.5	-3.1 ± 5.8
	TC0603 duplicate	1	0.04	1.4E-06	0.864880 ± 3	0.467113 ± 2	0.864890 ± 6	0.467120 ± 3	0.864887 ± 3	0.467116 ± 2	-7.3 ± 4.0	2.1 ± 3.4
	CT02-358	1	0.04	1.7E-06	0.864876 ± 6	0.467111 ± 3	0.864895 ± 12	0.467119 ± 6	0.864885 ± 6	0.467114 ± 3	-9.4 ± 7.4	-2.8 ± 7.2
	CT02-358 duplicate	1	0.02	1.0E-06	0.864881 ± 3	0.467113 ± 1	0.864894 ± 4	0.467119 ± 2	0.864887 ± 3	0.467116 ± 1	-7.4 ± 3.0	1.9 ± 2.6
	CT02-548	1	0.03	1.5E-06	0.864878 ± 4	0.467114 ± 2	0.864882 ± 7	0.467118 ± 3	0.864880 ± 4	0.467116 ± 2	-15.2 ± 4.6	1.1 ± 3.7
Pilbara Craton	AH-25	1	0.03	3.2E-07	0.864892 ± 3	0.467113 ± 1	0.864917 ± 6	0.467123 ± 3	0.864904 ± 4	0.467118 ± 2	13.1 ± 4.1	5.2 ± 3.5
	AH-26	1	0.07	4.4E-07	0.864902 ± 4	0.467116 ± 2	0.864911 ± 7	0.467117 ± 3	0.864906 ± 4	0.467116 ± 2	15.3 ± 4.6	2.4 ± 3.7
	Alfa Aesar W standards	1	0.01	1.5E-06	0.864890 ± 3	0.467115 ± 1	0.864891 ± 6	0.467116 ± 3	0.864892 ± 3	0.467117 ± 1	-1.3 ± 3.5	2.9 ± 3.2
			0.01	5.8E-07	0.864892 ± 3	0.467114 ± 2	0.864899 ± 6	0.467118 ± 3	0.864895 ± 4	0.467116 ± 2	2.6 ± 4.3	1.4 ± 3.7
			0.01	9.1E-07	0.864888 ± 4	0.467114 ± 2	0.864901 ± 7	0.467116 ± 3	0.864893 ± 4	0.467115 ± 2	0.0 ± 4.3	0.0 ± 3.9
			0.01	1.2E-06	0.864892 ± 4	0.467115 ± 2	0.864901 ± 7	0.467120 ± 3	0.864895 ± 4	0.467117 ± 2	1.8 ± 4.9	4.5 ± 4.3
			0.01	5.4E-07	0.864885 ± 5	0.467111 ± 2	0.864897 ± 9	0.467117 ± 4	0.864892 ± 5	0.467114 ± 2	-1.6 ± 5.9	-2.5 ± 5.3
			0.02	1.2E-06	0.864880 ± 4	0.467111 ± 2	0.864898 ± 8	0.467122 ± 4	0.864890 ± 4	0.467114 ± 2	-3.9 ± 5.1	-2.6 ± 4.4
			0.03	1.1E-07	0.864886 ± 5	0.467113 ± 2	0.864892 ± 10	0.467118 ± 5	0.864892 ± 5	0.467116 ± 2	-1.5 ± 6.0	2.2 ± 5.0
			0.02	8.9E-07	0.864882 ± 5	0.467108 ± 2	0.864900 ± 10	0.467119 ± 4	0.864890 ± 6	0.467114 ± 3	-3.5 ± 6.6	-2.5 ± 5.4
			0.02	2.5E-07	0.864887 ± 4	0.467110 ± 2	0.864906 ± 8	0.467116 ± 4	0.864894 ± 5	0.467114 ± 2	1.4 ± 5.4	-3.6 ± 4.4
			0.02	1.8E-06	0.864885 ± 4	0.467111 ± 2	0.864900 ± 7	0.467121 ± 4	0.864894 ± 4	0.467116 ± 2	1.4 ± 4.8	2.2 ± 4.3
			0.01	6.0E-07	0.864893 ± 4	0.467113 ± 2	0.864900 ± 7	0.467116 ± 3	0.864896 ± 4	0.467114 ± 2	3.6 ± 4.6	-1.8 ± 3.9
			0.02	9.8E-07	0.864885 ± 4	0.467112 ± 2	0.864900 ± 7	0.467117 ± 3	0.864894 ± 4	0.467115 ± 2	1.0 ± 4.6	0.0 ± 4.0

Table S-4 ***(continued)*** Detailed W isotope data for the Réunion Island, the Kerguelen Archipelago and the Pilbara Craton samples.

Location	Sample	Analytical session	$^{185}Re/^{184}W$	$^{181}Ta/^{184}W$	*Static line 1*		*Static line 2*		*Mean line 1 + line 2*		$\mu^{182}W$	$\mu^{183}W$
					$^{182}W/^{184}W$	$^{183}W/^{184}W$	$^{182}W/^{184}W$	$^{183}W/^{184}W$	$^{182}W/^{184}W$	$^{183}W/^{184}W$		
	Alfa Aesar W standards	2	0.02	-5.2E-06	0.864893 ± 7	0.467114 ± 3	0.864906 ± 6	0.467115 ± 3	0.864900 ± 5	0.467115 ± 2	-0.9 ± 5.3	-5.5 ± 4.6
			0.04	-4.0E-06	0.864904 ± 7	0.467123 ± 3	0.864899 ± 7	0.467115 ± 3	0.864903 ± 5	0.467118 ± 2	2.4 ± 5.8	2.8 ± 4.6
			0.10	-2.8E-06	0.864906 ± 6	0.467117 ± 3	0.864903 ± 6	0.467119 ± 3	0.864905 ± 4	0.467118 ± 2	5.0 ± 5.0	2.2 ± 4.5
			0.05	-2.5E-06	0.864898 ± 6	0.467115 ± 3	0.864902 ± 6	0.467117 ± 3	0.864902 ± 4	0.467116 ± 2	1.6 ± 4.8	-2.2 ± 4.2
			0.07	-3.7E-06	0.864898 ± 4	0.467121 ± 2	0.864903 ± 5	0.467114 ± 2	0.864899 ± 3	0.467117 ± 2	-2.0 ± 3.6	-0.5 ± 3.3
			0.04	-4.1E-06	0.864896 ± 4	0.467118 ± 2	0.864904 ± 4	0.467115 ± 2	0.864899 ± 3	0.467117 ± 1	-2.6 ± 3.0	-0.4 ± 2.8
			0.03	-1.9E-06	0.864893 ± 7	0.467118 ± 3	0.864904 ± 7	0.467120 ± 3	0.864898 ± 4	0.467119 ± 2	-3.5 ± 5.2	3.6 ± 4.4

Notes: Precision for isotope ratios is given is ± 2 s.e. on last decimals place. Tungsten isotope ratios are also reported in μ values ± 2 s.e. (ppm) relative to the W standard measured during the same analytical session as the samples.

Supplementary Figures

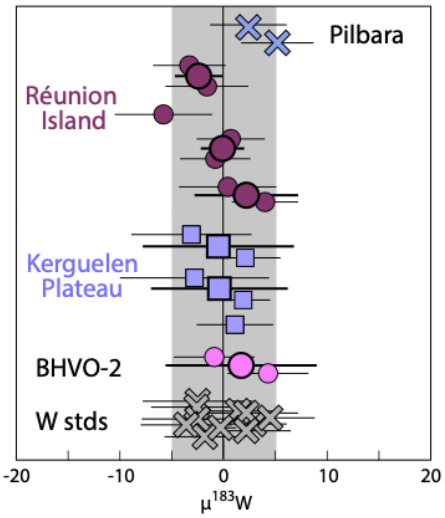

Figure S-1 $^{183}W/^{184}W$ data obtained in this study, shown as $\mu^{183}W$ values, which are relative deviations of the W isotope composition of the samples from the terrestrial standard in parts per million (ppm) ($\mu^{183}W = [(^{183}W/^{184}W)_{sample}/(^{183}W/^{184}W)_{standard}]-1)*10^6$). Small symbols are individual analysis of samples with errors in 2 s.e.; larger symbols show the average of the different duplicates, with respective 2 s.d. errors. The shaded area represents the reproducibility obtained (2 s.d.) on repeated measurements of the Alfa Aesar W standard.

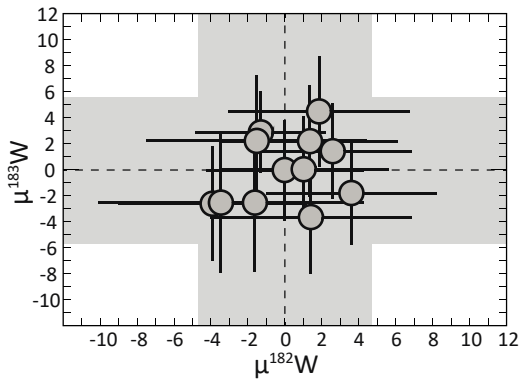

Figure S-2 $\mu^{182}W$ *vs.* $\mu^{183}W$ values for tungsten standard measurements performed in this study. The shaded area represents the reproducibility obtained (2 s.d.) on repeated measurements of the Alfa Aesar W standard.

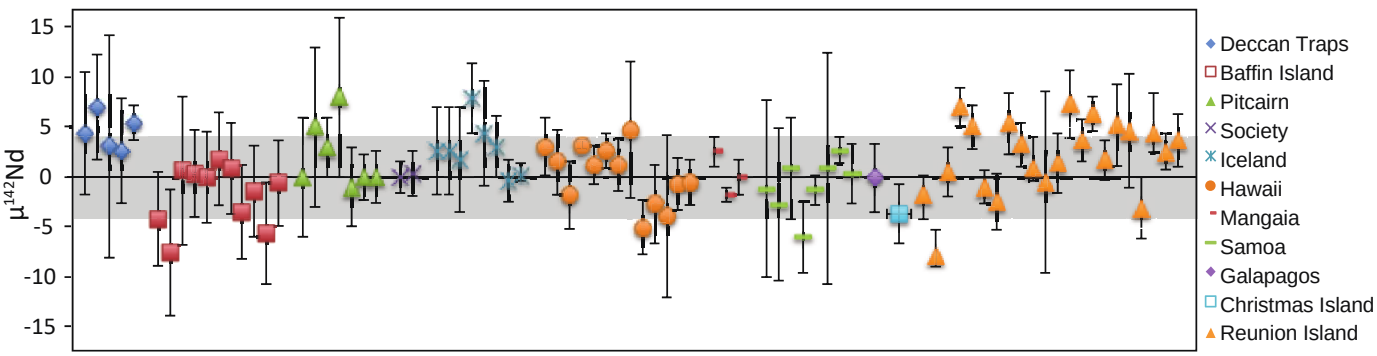

Figure S-3 $^{142}Nd/^{144}Nd$ data of plume-related rock samples. $^{142}Nd/^{144}Nd$ is shown as $\mu^{142}Nd$ values, which is the deviation in ppm from the Nd terrestrial standard ($\mu^{142}Nd = 0$). The shaded area represents the typical reproducibility obtained (2 s.d.) obtained on repeated measurements of the Nd terrestrial standard. Data from Andreasen *et al.* (2008), Boyet and Carlson (2006), Caro *et al.,* (2006), de Leeuw *et al.* (2017), Garçon *et al.* (2018), Horan *et al.* (2018), Jackson *et al.* (2012), Murphy *et al.* (2010), and Peters *et al.* (2018).

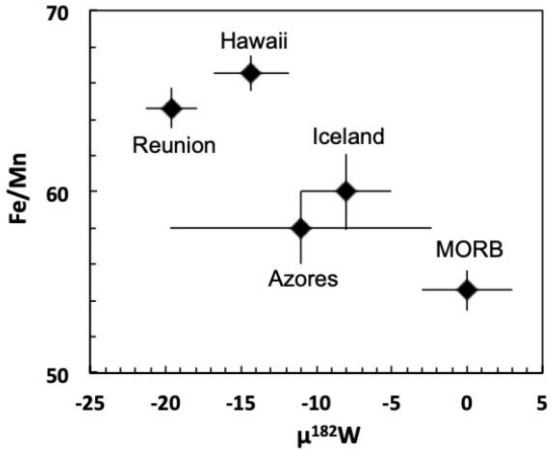

Figure S-4 Comparison of the potential core-mantle interaction tracer Fe/Mn in OIB suites that have been analysed for $\mu^{182}W$. Only averages of the lowest $\mu^{182}W$ for each of the OIB localities are shown (see Fig. 2 of the main manuscript for sources). Average of Fe/Mn ratios reported for MORB, Iceland, Pico (Azores), Reunion, and Hawaii (Humayun *et al.*, 2004; Qin and Humayun, 2008; Vlastélic *et al,* 2006; Humayun, *unpublished*). For Azorean samples shown, $\mu^{182}W$ and Fe/Mn are both limited to Pico Island lavas, which do not represent the same samples but represent the same lava flows for most samples. For Hawaii, all three tracers were measured on at least some of the same samples, while for Iceland Fe/Mn ratios were measured on the same samples.

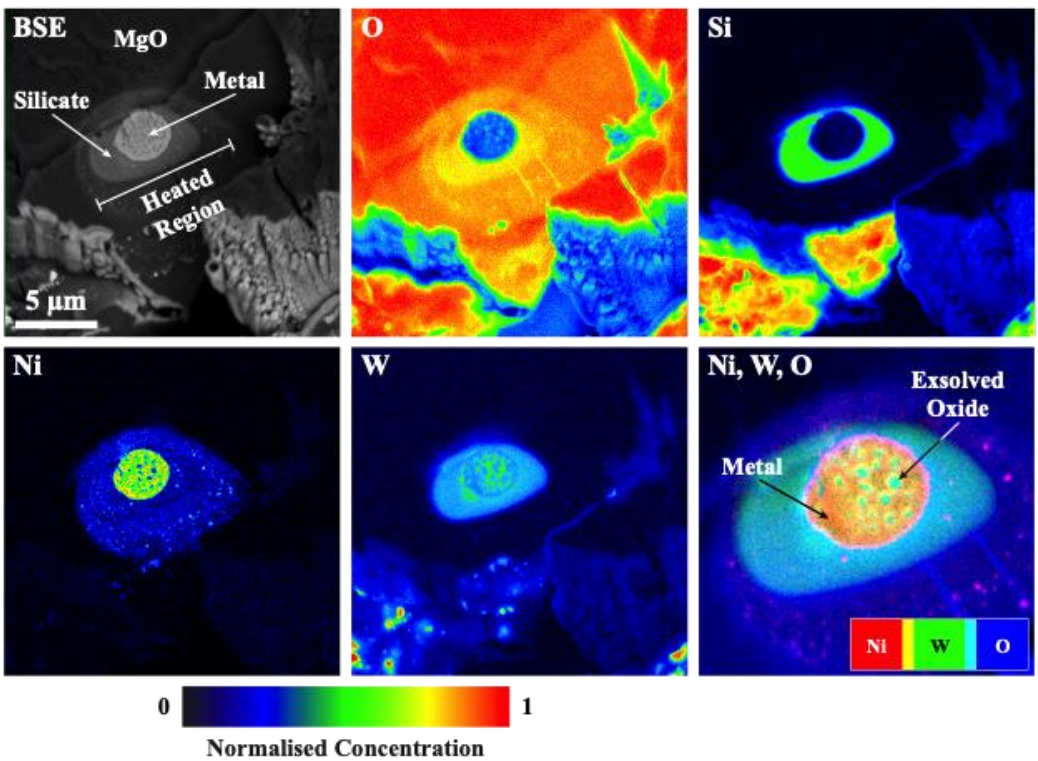

Figure S-5 BSE image and WDS maps for a LH-DAC experiment quenched from ~24 GPa and 3250 K. Within the quenched metal phase at the centre of the heated region, Si, O, and W concentrations are broadly correlated, suggesting they partition preferentially into the oxide phase which is exsolved when the sample is quenched (darker grey blebs in the BSE image). In contrast, Ni remains more concentrated in the metal phase. The final panel combines data for W, Ni, and O, in order to better highlight the concentration of W in the exsolved oxide phase.

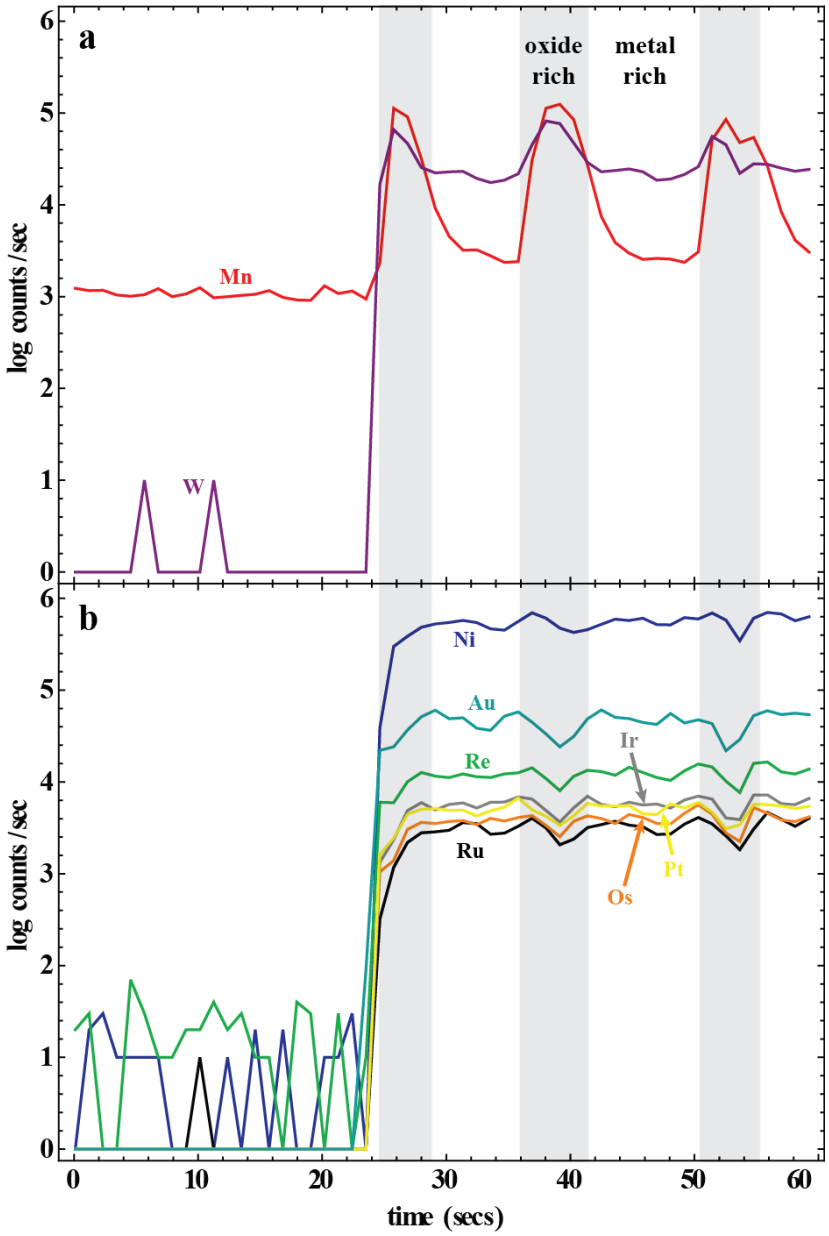

Figure S-6 Time-resolved LA-ICPMS spectra for **(a)** W, Mn and **(b)** the HSEs. Spectra represent a line analysis over a portion of the sample that contained varying amounts of exsolved oxide – leading to heterogeneity in the time-resolved spectrum. Regions of high W and Mn counts/sec represent ablation of an oxide rich part of the sample. Coincident with these high counts/sec regions in the W and Mn spectra are low counts/sec dips in the HSE spectra. This suggests the exsolved oxide phase is enriched in W and Mn, but depleted in the HSEs. The time-resolved spectrum for Ni displays less variation than the other elements, but appears to follow the HSE behaviour. Results from Bennett *et al*. (2014).

Supplementary Information References

Andreasen, R., Sharma, M., Subbarao, K.V., Viladkar, S.G. (2008) Where on Earth is the enriched Hadean reservoir?. *Earth and Planetary Science Letters* 266, 14-28.

Archer, G.J., Mundl, A., Walker, R.J., Worsham, E.A., Bermingham, K.R. (2017) High-precision analysis of $^{182}W/^{184}W$ and $^{183}W/^{184}W$ by negative thermal ionization mass spectrometry: Per-integration oxide corrections using measured $^{18}O/^{16}O$. *International Journal of Mass Spectrometry* 414, 80-86.

Bennett, N.R., Fei, Y. (2014) Element redistribution in Fe-Ni-O alloys by a thermal gradient: implications for siderophile element partitioning and during core-formation and crystallization. *AGU Fall Meeting Abstracts*, DI51A-4344.

Boyet, M., Carlson, R.W. (2006) A new geochemical model for the Earth's mantle inferred from $^{146}Sm–^{142}Nd$ systematics. *Earth and Planetary Science Letters* 250, 254-268.

Breton, T., Quitté, G. (2014) High-precision measurements of tungsten stable isotopes and application to earth sciences. *Journal of Analytical Atomic Spectrometry* 29, 2284-2293.

Campbell, A.J., Danielson, L., Righter, K., Seagle, C. T., Wang, Y., Prakapenka, V.B. (2009). High pressure effects on the iron–iron oxide and nickel–nickel oxide oxygen fugacity buffers. *Earth and Planetary Science Letters* 286, 556-564.

Caro, G., Bourdon, B., Birck, J.L., Moorbath, S. (2006) High-precision $^{142}Nd/^{144}Nd$ measurements in terrestrial rocks: constraints on the early differentiation of the Earth's mantle. *Geochimica et Cosmochimica Acta* 70, 164-191.

Chabot, N.L., Wollack, E.A., Humayun, M., Shank, E.M. (2015) The effect of oxygen as a light element in metallic liquids on partitioning behavior. *Meteoritics & Planetary Science* 50, 530-546.

Cook, D.L., Schönbächler, M. (2016) High-precision measurement of W isotopes in Fe–Ni alloy and the effects from the nuclear field shift. *Journal of Analytical Atomic Spectrometry* 31, 1400-1405.

de Leeuw, G.A.M., Ellam, R.M., Stuart, F.M., Carlson, R.W. (2017) $^{142}Nd/^{144}Nd$ inferences on the nature and origin of the source of high $^{3}He/^{4}He$ magmas. *Earth and Planetary Science Letters* 472, 62-68.

Doucet, S., Scoates, J.S., Weis, D., Giret, A. (2005) Constraining the components of the Kerguelen mantle plume: A Hf-Pb-Sr-Nd isotopic study of picrites and high-MgO basalts from the Kerguelen Archipelago. *Geochemistry, Geophysics, Geosystems* 6.

Doucet, S., Moreira, M., Weis, D., Scoates, J.S., Giret, A., Allegre, C. (2006) Primitive neon and helium isotopic compositions of high-MgO basalts from the Kerguelen Archipelago, Indian Ocean. *Earth and Planetary Science Letters* 241, 65-79.

Fortenfant, S.S., Rubie, D.C., Reid, J., Dalpé, C., Capmas, F., Gessmann, C.K. (2003) Partitioning of Re and Os between liquid metal and magnesiowustite at high pressure. *Physics of the Earth and Planetary Interiors* 139, 77-91.

Garçon, M., Boyet, M., Carlson, R.W., Horan, M.F., Auclair, D., Mock, T.D. (2018) Factors influencing the precision and accuracy of Nd isotope measurements by thermal ionization mass spectrometry. *Chemical Geology* 476, 493-514.

Gurioli, L., Muro, A., Vlastélic, I., Moune, S., Thivet, S., Valer, M., Villeneuve, N., Boudoire, G., Peltier, A., Bachèlery, P., Ferrazzini, V., Métrich, N., Benbakkar, M., Cluzel, N., Constantin, C., Devidal, J.-L., Fonquernie, C., Hénot, J.-M. (2017) Integrating field, textural, and geochemical monitoring to track eruption triggers and dynamics: a case study from Piton de la Fournaise. *Solid Earth* 9, 431-455.

Horan, M.F., Carlson, R.W., Walker, R.J., Jackson, M., Garçon, M., Norman, M. (2018) Tracking Hadean processes in modern basalts with 142-Neodymium. *Earth and Planetary Science Letters* 484, 184-191.

Huang, S., Humayun, M., Frey, F.A. (2007) Iron/manganese ratio and manganese content in shield lavas from Ko'olau Volcano, Hawai'i. *Geochimica et Cosmochimica Acta* 71, 4557-4569.

Humayun, M., Qin, L., Norman, M.D. (2004) Geochemical evidence for excess iron in the mantle beneath Hawaii. *Science* 306, 91-94.

Ingle, S., Weis, D., Doucet, S., Mattielli, N. (2003). Hf isotope constraints on mantle sources and shallow-level contaminants during Kerguelen hot spot activity since~ 120 Ma. *Geochemistry, Geophysics, Geosystems*, 4(8).

Jackson, M.G., Carlson, R.W. (2012) Homogeneous superchondritic $^{142}Nd/^{144}Nd$ in the mid-ocean ridge basalt and ocean island basalt mantle. *Geochemistry, Geophysics, Geosystems* 13.

Kranendonk, M.J.V., Hickman, A.H., Smithies, R.H., Nelson, D.R., Pike, G. (2002) Geology and tectonic evolution of the archean North Pilbara terrain, Pilbara Craton, Western Australia. *Economic Geology* 97, 695-732.

Kruijer, T.S., Kleine, T. (2018) No ^{182}W excess in the Ontong Java Plateau source. *Chemical Geology* 485, 24-31.

Mundl, A., Touboul, M., Jackson, M.G., Day, J.M., Kurz, M.D., Lekic, V., Helz, R.T., Walker, R.J. (2017) Tungsten-182 heterogeneity in modern ocean island basalts. *Science* 356, 66-69.

Murphy, D.T., Brandon, A.D., Debaille, V., Burgess, R., Ballentine, C. (2010) In search of a hidden long-term isolated sub-chondritic $^{142}Nd/^{144}Nd$ reservoir in the deep mantle: Implications for the Nd isotope systematics of the Earth. *Geochimica et Cosmochimica Acta* 74, 738-750.

Peters, B.J., Carlson, R.W., Day, J.M., Horan, M.F. (2018) Hadean silicate differentiation preserved by anomalous $^{142}Nd/^{144}Nd$ ratios in the Réunion hotspot source. *Nature* 555, 89.

Qin, L., Humayun, M. (2008) The Fe/Mn ratio in MORB and OIB determined by ICP-MS. *Geochimica et Cosmochimica Acta* 72, 1660-1677.

Shofner, G.A. (2011) High Pressure Redox Geochemistry of Tungsten in Metal-Silicate Systems : Implications for Core Formation in the Earth. PhD Thesis, University of Maryland College Park.

Shofner, G.A., Campbell, A.J., Danielson, L.R., Righter, K., Fischer, R.A., Wang, Y., Prakapenka, V. (2016) The W-WO_2 oxygen fugacity buffer at high pressure and temperature: Implications for fO_2 buffering and metal-silicate partitioning. *American Mineralogist* 101, 211-221.

Sobolev, A.V., Hofmann, A.W., Kuzmin, D.V., Yaxley, G.M., Arndt, N.T., Chung, S.L., Danyushevsky, L.V., Elliott, T., Frey, F.A., Garcia, M.O., Gurenko, A.A., Kamenetsky, V.S., Kerr, A.C., Krivolutskaya, N.A., Matvienkov, V.V., Nikogosian, I.K., Rocholl, A., Sigurdsson, I.A., Sushchevskaya, N.M., Teklay, M. (2007) The amount of recycled crust in sources of mantle-derived melts. *Science* 316, 412-417.

Thibault, Y., Walter, M. J. (1995) The influence of pressure and temperature on the metal-silicate partition coefficients of nickel and cobalt in a model C1 chondrite and implications for metal segregation in a deep magma ocean. *Geochimica et Cosmochimica Acta*, 59, 991-1002.

Trieloff, M., Kunz, J. (2005) Isotope systematics of noble gases in the Earth's mantle: possible sources of primordial isotopes and implications for mantle structure. *Physics of the Earth and Planetary Interiors* 148, 13-38.

Vlastélic, I., Lewin, E., Staudacher, T. (2006) Th/U and other geochemical evidence for the Reunion plume sampling a less differentiated mantle domain. *Earth and Planetary Science Letters* 248, 379-393.

Vlastélic, I., Deniel, C., Bosq, C., Télouk, P., Boivin, P., Bachèlery, P., Famin, V., Staudacher, T. (2009) Pb isotope geochemistry of Piton de la Fournaise historical lavas. *Journal of Volcanology and Geothermal Research* 184, 63-78.

Vlastélic, I., Menard, G., Gannoun, A., Piro, J.L., Staudacher, T., Famin, V. (2013) Magma degassing during the April 2007 collapse of Piton de la Fournaise: the record of

semi-volatile trace elements (Li, B, Cu, In, Sn, Cd, Re, Tl, Bi). *Journal of Volcanology and Geothermal Research* 254, 94-107.

Vlastélic, I., Di Muro, A., Bachèlery, P., Gurioli, L., Auclair, D., Gannoun, A. (2018) Control of source fertility on the eruptive activity of Piton de la Fournaise volcano, La Réunion. *Scientific reports* 8, 14478.

Völkening, J., Köppe, M., Heumann, K.G. (1991) Tungsten isotope ratio determinations by negative thermal ionization mass spectrometry. *International Journal of Mass Spectrometry and Ion Processes* 107, 361-368.

Wiemer, D., Schrank, C.E., Murphy, D.T., Hickman, A.H. (2016) Lithostratigraphy and structure of the early Archaean Doolena Gap greenstone belt, East Pilbara Terrane, Western Australia. *Precambrian Research* 282, 121-138.

Woodhead, J. (2002) A simple method for obtaining highly accurate Pb isotope data by MC-ICP-MS. *Journal of Analytical Atomic Spectrometry* 17, 1381-1385.